Journal of Structural Biology **132,** 112–122 (2000)
doi:10.1006/jsbi.2000.4307, available online at http://www.idealibrary.com on IDEAL®

Secondary Structure of Chorion Proteins of the Teleostean Fish *Dentex dentex* by ATR FT-IR and FT-Raman Spectroscopy

V. A. Iconomidou,* D. G. Chryssikos,† V. Gionis,† M. A. Pavlidis,‡ A. Paipetis,† and S. J. Hamodrakas*

**Department of Cell Biology and Biophysics, Faculty of Biology, University of Athens, Athens 157 01, Greece; †Institute of Theoretical and Physical Chemistry, National Hellenic Research Foundation, Athens 116 35, Greece; and ‡Institute of Marine Biology of Crete, Heraklion 71003, Crete, Greece*

Received May 8, 2000, and in revised form July 21, 2000; published online December 7, 2000

FT-Raman spectroscopy and ATR-IR spectroscopy were applied to study the secondary structure of the eggshell (chorion) proteins of the teleostean fish *Dentex dentex*. Raman and IR spectra clearly indicate an abundance of antiparallel β-pleated sheet conformation in chorion proteins. This finding is further supported by analysis of the vibrational data by regression techniques and deconvolution procedures. Thus, the common morphological characteristics of *D. dentex, Salmo gairdneri,* and other teleostean fish chorions may be explained on the basis of common secondary structure features of their constituent proteins. A detailed understanding of the interactions that dictate the self-assembly of fish chorion proteins to form the fish eggshell awaits determination of amino acid sequences.

Key Words: **ATR-IR spectroscopy; fish eggshell (chorion); FT-Raman spectroscopy; helicoidal architecture; β-pleated sheet; scanning microscopy.**

INTRODUCTION

Teleost fishes develop mature eggs enclosed in a hard and complex eggshell (chorion), which is formed by protein components organized into a complex structure. This structure plays an essential role in controlling the relation between the external and the internal egg environments: It allows for respiratory gas diffusion, provides mechanical protection and thermal insulation, and permits sperm entry (Hamodrakas, 1992).

The fish chorion is a helicoidal composite of protein fibers in a protein matrix. It consists of parallel planes or sheets of fibrils (mono- or polymolecular) in a spiral arrangement. Within individual planes, the fibrils are oriented more or less parallel to one another. Between successive planes the fibril direction rotates progressively, thus giving rise to a helix, with its axis perpendicular to the planes (Bouligand, 1972; Grierson and Neville, 1981; Hamodrakas, 1992). The close structural analogy between the (usually extracellular) helicoidal biological structures and the cholesteric liquid crystals probably suggests that several tissues and organelles self-assemble according to a mechanism that is very similar to the process allowing materials to form liquid crystals (Neville, 1975; Bouligand, 1978b).

Self-assembling systems are important in biology as they are economical in energy terms, requiring neither enzymatic control nor the expenditure of energy-rich bonds. They are particularly appropriate for building extracellular skeletal structures (Neville, 1986; Bouligand, 1978a,b), and therefore it is important to determine the molecular mechanisms that lead to their formation.

The principles governing the self-assembly of protein molecules into helicoidal proteinaceous extracellular structures should be based on simple rules of packing of protein molecules. These are known to depend on secondary structure element interactions (α-helices and β-sheets), constituents of the protein molecules or domains (Schultz and Schirmer, 1978). Therefore, the first step toward unraveling the modes of interaction of protein molecules leading to the formation of helicoidal proteinaceous eggshells should be the determination of chorion protein secondary structure.

In this respect, fish egg chorions, in particular, are relatively favorable specimens for vibrational spectroscopic studies. They consist almost exclusively of protein (Hamodrakas *et al.*, 1987; Papadopoulou *et al.*, 1996) and function as essentially dry shells. The absence of major admixtures, such as chitin or other carbohydrates, minimizes interference from other than protein vibrations. These features permit the analysis of intact chorion structure, as opposed to protein extracts, ensuring that the structural features observed reflect the physiological state.

Some years ago, intact chorions of the teleostean

1047-8477/00 $35.00

fish *Salmo gairdneri* were investigated by laser-Raman and infrared spectroscopy (Hamodrakas *et al.*, 1987; Papadopoulou *et al.*, 1996). These studies indicated that the β-pleated sheet is the molecular conformation that dictates the organization of protein macromolecules into fibrils and of fibrils into a proteinaceous eggshell with a helicoidal architecture.

The generalization of this finding requires the investigation of more helicoidal chorions, and the present work contributes toward the determination of the secondary structure features of chorion proteins of another teleostean fish, *Dentex dentex*.

MATERIALS AND METHODS

Sample preparation. Spawned (fertilized) eggs of *D. dentex* were obtained from the I.M.B.C. (Institute of Marine Biology of Crete, Heraclion, Crete, Greece).

The eggshells were cut in half with needles and forceps and washed thoroughly several times with distilled water in a sonicator to remove the newly formed embryo and other remnants. They were then thoroughly dried (3- to 4-s exposure) under an infrared emitter bulb. This process produces slightly better quality spectra than from air-dried samples.

Scanning electron microscopy. All dried half-chorions were stored in a vacuum dessicator at room temperature. They were mounted on silver stubs, with double-sided adhesive tape. Secured to the stubs, the samples were coated with gold in a sputter coater with an 18-nm coat. Samples were examined under a NOVASCAN 30 Microvid scanning electron microscope operating at 10 kV. Image processing was performed utilizing the program Image Slave 2.14.

FT-Raman. Sample preparation for Raman measurements involved pressing several eggshells into the 2-mm cavity of a standard aluminum holder. Raman spectra were obtained on a Fourier-transform instrument (Bruker RFS 100) employing for excitation ca. 400 mW of the Nd:YAG 1064-nm line in a backscattering geometry. Excitation in the near-infrared greatly reduces the fluorescence of the sample and eliminates the need for prolonged laser annealing, which is necessary if excitation in the visible is employed instead. The resolution was 8 cm^{-1} and the total acquisition time was ca. 10 h (10 000 scans). The interferograms were Fourier-transformed in 1-h acquisition time segments, in order to allow for the detection of time-dependent phenomena (sample degradation, luminescence, bleaching, etc). Subsequently, the spectra were averaged and the standard deviation (σ) was calculated.

Attenuated total reflectance-infrared spectroscopy (ATR-IR). Infrared spectra were obtained at a resolution of 2 cm^{-1}, on a Fourier-transform vacuum instrument (Bruker IFS 113v), equipped with a 45° KRS5 Attenuated Total Reflectance accessory. Internal reflection spectroscopy presents several advantages compared to the more common KBr dispersion technique (de Jongh *et al.*, 1996). Having a penetration depth of ca. 2 μm (1000 cm^{-1}, KRS5, 45°), ATR is free of saturation effects that may be present in the transmission spectra of thicker chorions. Furthermore, the choice of the ATR technique was dictated by the need to exclude any possible spectroscopic and chemical interactions between the sample and the dispersing medium. In the literature, ATR-IR has been employed for solutions of proteins, or for thin films deposited directly on the ATR crystal by evaporation of the solvent (de Jongh *et al.*, 1996; Fu *et al.*, 1994; Fink and Gendreau, 1984; Singh and Fuller, 1991; Jackobsen and Wasacz, 1990; Kim *et al.*, 1998). In the present investigation, several eggshells were placed on the surface of the KRS5 element and kept in place by tightening of the metal plate holder. Fifteen 400-scan spectra have been collected and averaged to improve the S/N ratio. The spectra are corrected for the effect of wavelength on the penetration depth ($pd \propto \lambda$). The corresponding effect of the (frequency-dependent) refractive index (n) of chorion samples was not taken into account due to the lack of relevant data.

Postrun computations of the spectra. The Raman scattering and infrared ATR absorption peak maxima were determined from the minima in the second derivative of the corresponding spectra. Derivatives were computed analytically using routines of the OPUS/OS2 software and included smoothing by the Savitzky–Golay algorithm over ± 8 cm^{-1} around each data point (Savitsky and Golay, 1964). Smoothing over narrower ranges resulted in a deterioration of the *S/N* ratio and did not increase the number of minima that could be determined with confidence.

Analysis of the infrared and Raman spectra (amide I, II, and III regions) into component bands was performed via the OPUS (Bruker) and ORIGIN (MicroCal) routines, both operating on the basis of the Levenberg–Marquardt algorithm (Jacobs, 1977). Band positions, intensities, widths, and shapes (Gauss–Lorentz) were left as freely adjustable parameters. The number of component bands was fixed and equal to that determined from the second derivative spectra. To account for baseline effects when deconvoluting a particular spectral range (e.g., amide III), a broader frequency range was considered. This resulted in fitting both higher and lower frequency components (which are not of amide III origin). Subtracting the low- and high-frequency wings, respectively, of these component bands provided a very good estimate of the baseline in the frequency range of interest. The quality of the fit was evaluated first by the sum of the differences between the measured and the calculated spectra squared. In addition, a stricter criterion was applied involving the match of the second derivative of the calculated spectrum to that of the *raw* spectrum prior to any baseline correction manipulation. The integrated intensity of component bands of interest was subsequently normalized appropriately to yield the relative spectral contribution of the particular component. More details of this procedure are included under Results.

RESULTS

Ultrastructure of D. dentex Eggshell

Figure 1 shows the ultrastructure of an eggshell (chorion) from a fertilized egg of *D. dentex* under low magnification. The chorion is rather thin, ca. 3–4 μm, compared to chorions of eggs from other teleostean fishes. For example, the *Salmo gairdneri* chorion is ca. 25–30 μm (Papadopoulou *et al.*, 1996), whereas both the *Labrax labrax* and *Sparus aurata* chorions (our unpublished data) have a thickness of ca. 5–6 μm. The chorion consists of a small number of lamellae ($\sim$9–10), which indicates, though it does not prove a helicoidal architecture. Our transmission electron microscopy data (unpublished) verify the existence of a helicoidal architecture (see also Grierson and Neville, 1981).

Vibrational Spectra

The Raman and infrared spectra obtained from intact *D. dentex* chorions are shown in Figs. 2 and 3,

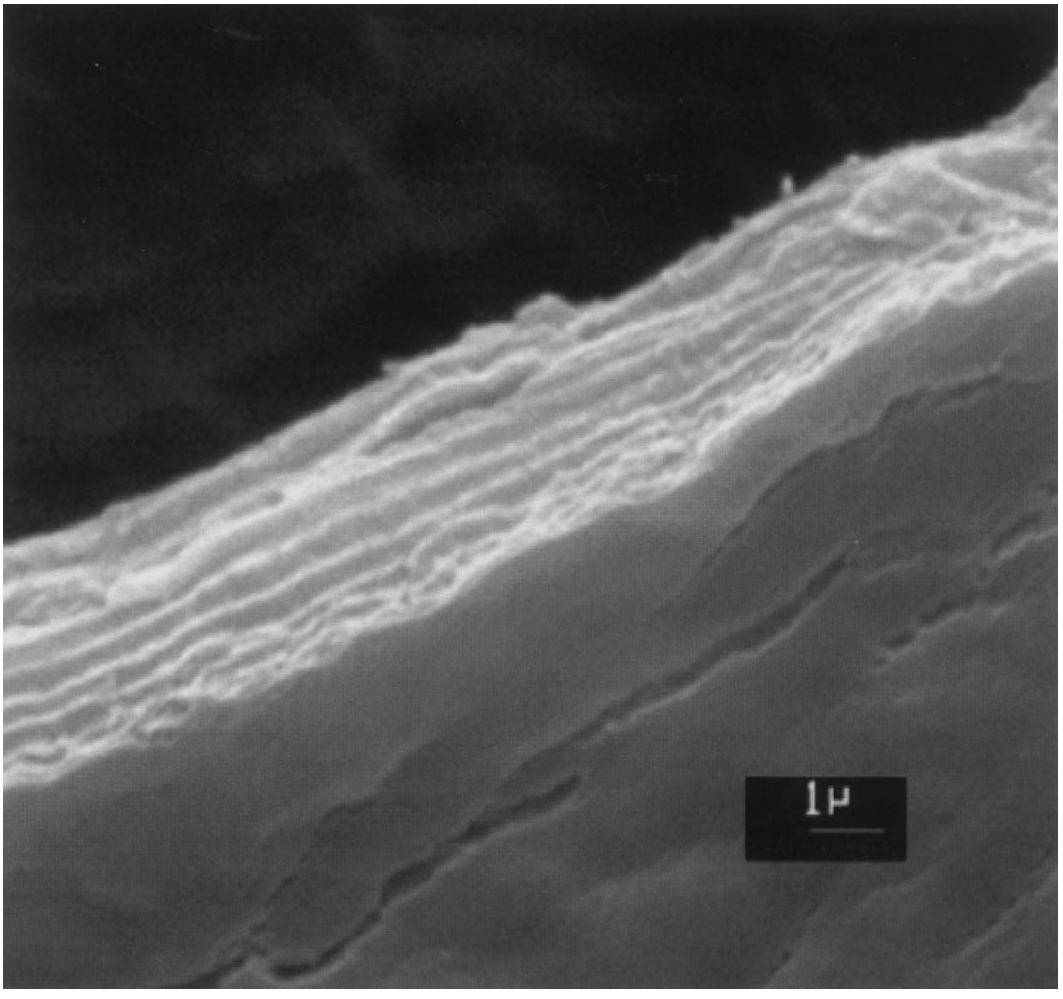

FIG. 1. Scanning electron micrograph from an oblique cross-sectional rip through an eggshell (chorion) of *Dentex dentex* showing inner surface regions and architecture. The eggshell was isolated from a fertilized egg. The lamellar structure of the eggshell is clearly discerned. Bar, 1 μm.

respectively. The error bar on the data equals 2σ, where σ is the standard deviation of the measurements. Inspection of Figs. 2 and 3 reveals that the vibrations of chorion proteins exhibit different activities in the Raman and infrared spectra, as expected from the different selection rules applicable for the two techniques. This fact results in significant differences in the apparent maxima and convoluted bandshapes. These differences are better discerned in Figs. 4 and 5, which include second-derivative spectra as well and indicate that nearly every vibrational mode is discernible in both spectra. The peak maxima in the two spectra, determined on the basis of their second derivatives, are compiled in Table I, together with the tentative assignments of the main spectral features.

No significant bands below 500 cm^{-1} were observed in the Raman spectra. Similarly, below ca. 1000 cm^{-1}, the infrared spectrum exhibits only a rather featureless broad envelope. Several bands are clearly assignable to side chain vibrations of amino acid residues, especially to the aromatic ring-containing Tyr, Trp, and Phe.

More specifically, the bands at 1033, 1003, and 622 cm^{-1} are ascribable to Phe, whereas the bands at 643, 830, 853, 1208, and 1612 cm^{-1} are most likely due to Tyr (Frushour and Koenig, 1975; Yu, 1977; Spiro and Gaber, 1977). The intensity ratio of the tyrosine doublet at 853 and 830 cm^{-1}, $R = I_{853}/I_{830}$, is sensitive to the nature of hydrogen bonding, or to the state of the ionization of the phenolic hydroxyl group, and has been used to identify "buried" and "exposed" Tyr moieties (Carey, 1982, and references therein). Tyr may also contribute to infrared absorption and Raman scattering at ca. 1270 and 1515–1500 cm^{-1} (Venyaminov and Kalnin,

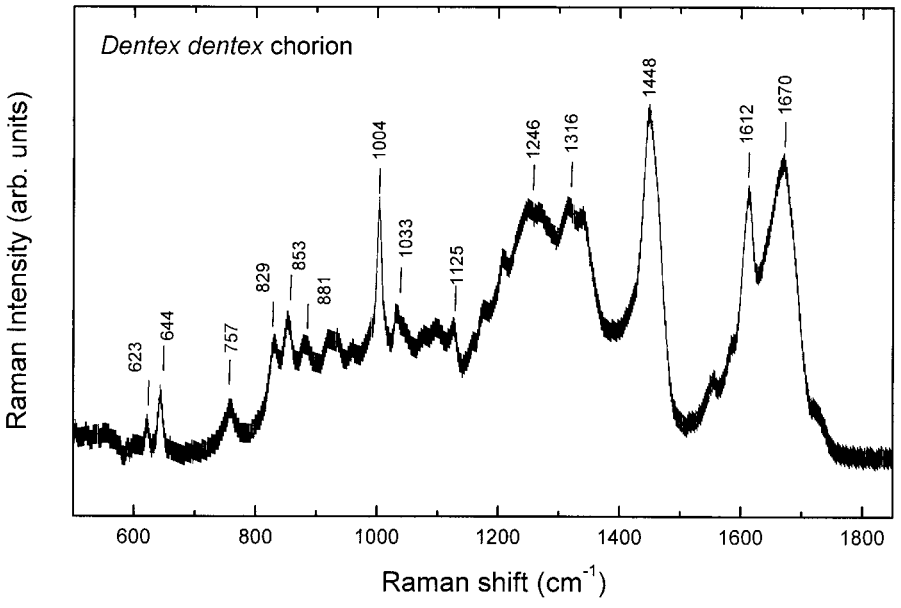

FIG. 2. Raman spectrum of the *Dentex dentex* chorion. Error bar equals 2σ.

1990a,b). The 643- and 1208-cm^{-1} bands may also involve vibrations of Phe. Also, the band at 1612 cm^{-1} may hide components due to Phe (1609 cm^{-1}) and Trp. Bands at 757 and 882 cm^{-1} are ascribable to Trp (Frushour and Koenig, 1975; Yu, 1977; Spiro and Gaber, 1977). The absence of a band at 1361 cm^{-1} suggests presumably that the Trp units are not exposed (Yu, 1977; Chen *et al.*, 1973).

Bands in the 500- to 550-cm^{-1} region are typically associated with the S–S stretching mode of the C–C–S–S–C–C structural unit of disulfide bonds (Frushour and Koenig, 1975; Yu, 1977; Spiro and Gaber, 1977).

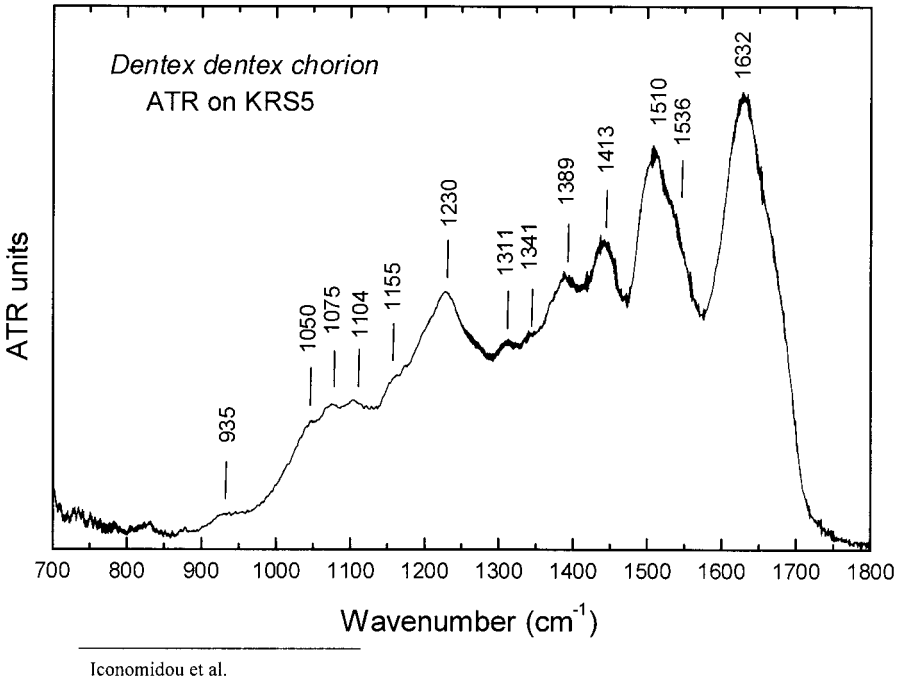

FIG. 3. Attenuated total reflectance infrared spectrum of the *Dentex dentex* chorion. Error bar equals 2σ.

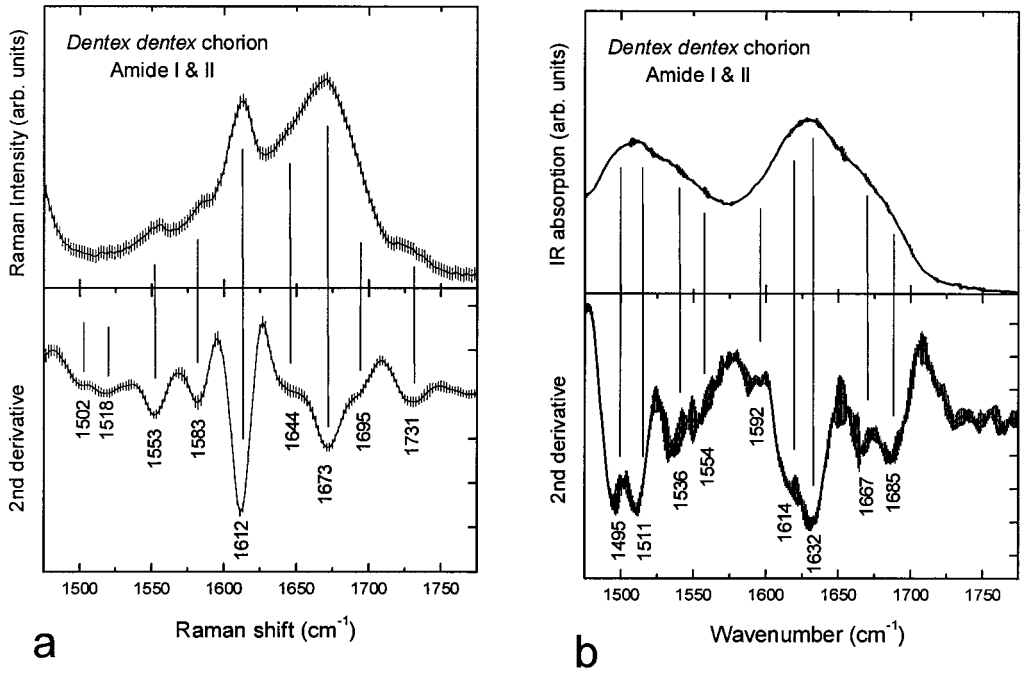

FIG. 4. Raman (a) and ATR-IR (b) spectra of the *Dentex dentex* chorion in the range 1475–1775 cm^{-1} (amide I and II). Second derivative spectra are included. Error bars are as in Fig. 2.

According to Edwards *et al.* (1998), the bands at 506 and 522 cm^{-1} in the FT-Raman spectra of keratins may be assigned to S–S bridges in g-g-g and g-g-t conformations, respectively. In the FT-Raman spectrum of *D. dentex* chorion two weak bands at 504 and 522 cm^{-1} are presumably of the same origin.

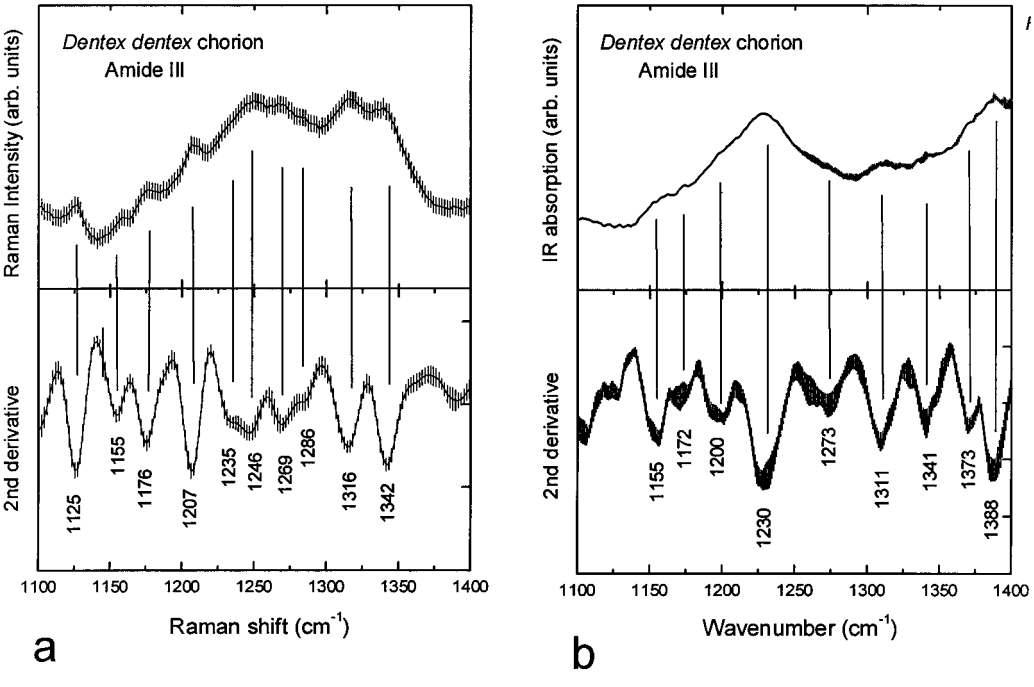

FIG. 5. Raman (a) and ATR-IR (b) spectra of the *Dentex dentex* chorion in the range 1100–1400 cm^{-1} (amide III). Second derivative spectra are included. Error bars are as in Fig. 2.

TABLE I

Main Raman (1800–450 cm^{-1}) and Infrared (1800–700 cm^{-1}) Peak Maxima of *D. dentex* Determined from the Second Derivative Spectra

Raman	Infrared	Assignment
1731	—	–COOH or lipid residue?
		Amide I
1695	1685	β-turns
1673		β-sheet
	1667	β-turn? random?
1644	**1632**	β-sheet
1612	1614	Tyr (Trp?)
1583	1592	
		Amide II
1553	1554	β-sheet, random?
	1536	β-sheet
1518	**1511**	Tyr
1502	1495	Tyr
1465		
1448		CH_2 deformation
1413	1413	CH_3 deformation
1390	**1389**	Buried Trp
	1371	
		Amide III
1342	1340	Trp? β-turns?
1316	**1311** (broad)	?
1286, 1269	1273	Random? β-turns?
1246, 1235	1230	β-sheet
1207	1200	Tyr, Phe
1176	1172	Tyr
1155	**1155**	
1125	1125	
	1110	
1100		
1050		
1033		Phe
1004		Phe
959		
935		
919		
881		Trp
853		Tyr doublet: buried
829		Tyr doublet: exposed
757		Trp
644		Tyr, Phe
623		Phe
522		S–S ggt
502		S–S ggg

Note. Strong bands are shown in boldface type. Tentative assignments are included. For details see text.

Armed with the identification of the vibrational signatures of the side groups, we can now focus our attention to the "amide" band envelopes, which are well-known indicators of secondary structural effects in proteins and polypeptides. Several papers review the relevant assignments of the Raman (Frushour and Koenig, 1975; Yu, 1977; Spiro and Gaber, 1977; Bandekar and Krimm, 1979; Carey and Salares, 1980; Carey, 1982) and IR (Venyaminov and Kalnin, 1990a,b; Singh *et al.*, 1990; Goormaghtigh *et al.*, 1990; Surewicz *et al.*, 1993; Haris and Chapman, 1995; Jackson and Mantsch, 1995; Griebenow *et al.*, 1999) spectra in the amide I, II, and III regions. These assignments are summarized for convenience in Table II.

In the amide I region (1600–1700 cm^{-1}) the Raman spectrum of the *D. dentex* chorion exhibits a well-defined maximum at 1673 cm^{-1}, whereas the ATR spectrum shows maximum absorption at 1632 cm^{-1}. Both maxima are typical of β-sheet structure. The presence of a band at 1667 cm^{-1} in the infrared spectrum is an indication for the presence of β-turns. There is some disagreement in the literature about the origin (β-turns or high-frequency component of antiparallel β-sheet) of bands in the region 1670–1695 cm^{-1} (Haris and Chapman, 1995 and references therein). The high-frequency 1685-cm^{-1} band (seen as a shoulder in the ATR spectrum and located at 1695 cm^{-1} in the FT-Raman spectrum) requires special attention. This band either is due to β-turns (probably joining strands of β-sheets, consequently part of the β-sheets themselves) or can be assigned to an antiparallel β-sheet. In proteins containing antiparallel β-sheets, a high-frequency β-sheet component that arises from transition dipole coupling is usually found at 50–70 cm^{-1} higher than the main β-sheet component (Jackson and Mantsch, 1995, and references therein).

Alltogether, the amide I spectra of intact *D. dentex* chorions strongly suggest that the most abundant secondary structure of chorion proteins is the β-sheet. The β-sheets are most probably antiparallel. The absence of strong bands at ca. 1650 cm^{-1} indicates that α-helical structures are not favored or remain below the detection limit of our techniques.

In the range 1400–1600 cm^{-1}, amide II vibrations are located at 1536 and 1554 cm^{-1} (better discerned from the infrared spectra). The positions of their maxima are consistent with the β-pleated sheet structural assignment. Although the amide II bands are considered of reduced diagnostic value,we note that the 1554-cm^{-1} component could also arise from random structures (see Table II). The strong 1510-cm^{-1} infrared band and the Raman shoulder at 1518 cm^{-1} are assigned to Tyr ring vibrations. However, it is interesting to note that the strong observed amide II band for poly-Gly I, an antiparallel β-pleated sheet structure, appears at 1517 cm^{-1} (Krimm and Bandekar, 1986).

The amide III range (1230–1320 cm^{-1}) is relatively free from side-group vibrations and, thus, highly diagnostic of secondary structure. Typically, the amide III range can be split in three regions, 1320–1280, 1270–1245, and 1245–1225 cm^{-1}, indicative of α-helices, random structures, and β-sheets, respectively (Fu *et al.*, 1994; Singh *et al.*, 1990).

TABLE II

Amide I, II, and III Infrared and Raman Wavenumber Ranges and Their Dependence on Secondary Structure

	α-helix		β-sheet		β-turns		Random/unordered		*D. dentex*	
	Infrared	Raman	Infrared	Raman	Infrared	Raman	Infrared	Raman	Infrared	Raman
Amide I	1644–1649[a]	1645–1663[c,d]	1691–1699[a]	1665–1680[c,d]	1662–1695[c]	1665,1690[c]	1650–1654[a]	1649–1665[d]	1685	1695
	or		or				or	(broad)	1667	1673
	1653–1660[b]		1610–1640[a,b,e]				1640–1650[b]		1632	1644
Amide II	1548–1553[a]	1545[c]	1563[a]	1560[c]		1560–1567[c]	1546–1553[a]		1554	1553
	or		or			1545–1555[c]				
	1519–1521[a]	1516[c]	1530–1535[a]	1535[c]					1536	
Amide III	1280–1317[f]	1260–1295[c]				1290–1330[c]			1340	1342
									1311	1316
										1286
									1273	1269
			1230–1245[f]	1230–1243[c,d,g]			1245–1270	1243–1249[d]		1246
									1230	1235

Note. Band maxima obtained from *D. dentex* chorions are included for comparison. Wavenumbers are in cm^{-1}.

[a] Venyaminov and Kalnin (1990).

[b] Griebenow *et al.* (1999).

[c] Orfanidou *et al.* (1995).

[d] Carey (1982).

[e] 1610–1625 intermolecular; 1630–1640 intramolecular (Griebenow *et al.*, 1999).

[f] Singh *et al.* (1990).

[g] Often appears split into 1233- and 1245-cm^{-1} components (Singh *et al.*, 1990).

More recently, the amide III range was split into four regions, 1330–1295, 1295–1270, 1270–1250, and 1250–1220 cm^{-1}, indicative of α-helix, β-turns, random coil, and β-sheet, respectively (Cai and Singh, 1999). The strongest amide III infrared bands of the *D. dentex* chorion are observed at 1311 and 1230 cm^{-1}. The latter is clearly due to β-sheet structure. A broader feature centered at ca. 1270 cm^{-1} is also observed in the infrared spectra. The corresponding Raman spectra exhibit a well-defined component at 1316 cm^{-1}, as well as doublets at 1235 and 1246 cm^{-1} and 1269 and 1286 cm^{-1}. Based on the aforementioned infrared assignments, the 1311-cm^{-1} band (Raman: 1316 cm^{-1}) ought to be attributed to α-helices. However, lacking firm evidence for such structures in the amide I spectra, we leave this band unassigned and plan to investigate a possible connection with β-turns (Krimm and Bandekar, 1986). The weak Raman feature at ca. 1286 cm^{-1} is presumably due to β-turns (Cai and Singh, 1999). To support these assignments, it is noted that the spectra of solid poly-glycine I and poly-L-alanine (two polypeptides that adopt the antiparallel β-sheet structure) are indeed characterized by Raman activity in the ranges 1290–1300 and 1230–1235 cm^{-1} (Carey and Salares, 1980). Both the infrared and the Raman spectra exhibit a strong feature at ca. 1340 cm^{-1}. This band falls outside the normally accepted range for amide III vibrations, although assignments of features similar to β-turns have been attempted (Bandekar and Krimm, 1979). Alternatively, we suggest that this feature could be attributed to a side-chain N–H vibration, which is sensitive to secondary structure. The splitting of the β-sheet mode at ca. 1240 cm^{-1} (Raman: 1235 and 1246 cm^{-1}) is not uncommon (Singh *et al.*, 1990). Finally, vibrational activity at ca. 1270 cm^{-1} in both the infrared and the Raman spectra is associated with the presence of unordered structures or β-turns.

Quantitative Estimates of Secondary Structure

There is rich spectroscopic literature on the quantification of the secondary structure of proteins on the basis of their infrared and Raman spectra. The quantitative methodologies can be grouped into two classes. The first class is of chemometric nature and involves the application of some kind of regression analysis [Raman: Williams and Dunker (1981), Hamodrakas *et al.* (1984), Williams (1986); infrared: Dousseau and Pézolet (1990), Lee *et al.* (1990), Sarver and Krueger (1991a, b)]. A database of reference spectra is required for which the secondary structure is accurately known by an independent technique (e.g., X-ray crystallography, circular dichroism). The spectra of both reference and unknown structures are subjected to the same pretreatment, which may involve the selection of the most appropriate frequency ranges, the subtraction of baseline and side-group contributions, smoothing, derivation, vector normalization, etc. A calibration method is then constructed correlating the spectroscopic activity with the secondary structure of the reference compounds. After a validation procedure

against a second set of reference spectra, the method can be applied to quantify the structure of unknown samples. Methods of this type are usually very powerful in yielding directly quantitative data, without the need for detailed spectral assignments, provided that the calibration and validation data sets are representative and accurate.

The second approach involves the deconvolution of the spectral range of interest (again usually after pretreatment) into component bands (Susi and Byler, 1986; Venyaminov and Kalnin, 1990a,b; Goormaghtigh *et al.*, 1990; Surewicz *et al.*, 1993 and references therein; Haris and Chapman, 1995; Griebenow *et al.*, 1999; Cai and Singh, 1999; to mention a few). The individual components need to be assigned to vibrational modes of specific structural entities. Yet, even if unambiguous assignments are possible, deconvolution yields only the relative contribution of each component band to the spectrum examined. Converting this information to quantitative structural results requires a renormalization of the fractional band areas that takes into account the respective (relative or absolute) extinction (or scattering) coefficients of the individual component bands (de Jongh *et al.*, 1996; Venyaminov and Kalnin, 1990a,b).

Along these lines, we have first analyzed the Raman amide I spectrum of the *D. dentex* chorion with the regression method described by Hamodrakas *et al.* (1984). This method, which is a modification of the method of Williams and Dunker (1981), employs a database of 15 known protein structures and yields a 6-component quantitative structural evaluation in terms of mono- and bihydrogen bonded α-helices, antiparallel and parallel β-sheets, β-turns, and undefined configurations (random coil). Based on this treatment the chorion proteins of *D. dentex* were found to consist of ca. 60% antiparallel β-pleated sheet, 30% β-turns, and 10% undefined structure (random coil). No significant participation of parallel β-sheets and helices was detected.

We should point out that: (a) the Raman basis set of 15 proteins contains two to three proteins approaching a β-sheet content of ca. 50%; (b) this reference set contains globular, water-soluble proteins only, whereas fish chorion proteins are structural proteins; and (c) the β-sheet content of structural proteins can be as high as 80% (Hamodrakas, 1992, and references therein). Therefore, we consider the results of the Raman chemometric analysis of semiquantitative value only.

Similarly, we have applied the singular value decomposition method of Sarver and Krueger (1991a,b) to the corresponding infrared amide I spectrum. The method is based on a database of 15 reference proteins in solution, and the structures are expressed in terms of total α-helix, β-sheet, β-turn, and other (random coil) percentage contributions. Based on this method, the structural description of the *D. dentex* chorion proteins is of qualitative value only: Large fractions of β-sheet are estimated together with moderate contributions from β-turn and other (random coil) structures. The fractions of the latter two components are counterbalanced by a negative fraction of α-helices. Attempts to vary spectral normalization and baseline subtraction resulted in extreme variation of the helix, β-turn, and random coil fractions. There are several reasons for this instability. Sarver and Krueger's method exhibits high efficiency for determining helices and β-sheets, but the correlation coefficients for turns and random coil structures are relatively poor. More importantly, the method is based on protein solution spectra from which a significant contribution of water was subtracted. Though the method appears to work well with infrared data obtained and treated in the same manner as the reference data, it is not calibrated to include spectra of dry solid proteins.

Having established a semiquantitative structural evaluation of the secondary structure estimates of chorion proteins with regression analysis techniques, we can now compare the results to those derived from spectral deconvolution. The details concerning the data pretreatment and spectral analysis employed are presented under Materials and Methods. In the following example, the infrared amide I vibrations are considered. To account correctly for background contributions, the spectrum is deconvoluted over a relatively broad frequency range (1520–1750 cm^{-1}). In addition to the three amide I bands and the two ring vibrations that are active between ca. 1600 and 1700 cm^{-1} (see Table I), five more components were input to account for the tailing-off of the amide II contributions, as well as for the high-frequency curvature of the background. The results of the deconvolution are shown in Fig. 6 and summarized in Table III. The three amide I components are found at 1635, 1664, and 1685 cm^{-1}, in good agreement with the corresponding minima in the second derivative at 1632, 1667, and 1685 cm^{-1} (Table I). The half-widths of the three component bands were found to be equal to 53, 27, and 33 cm^{-1}, respectively. At least the first bandwidth is unusually large and can be taken as the envelope of unresolved components in the range 1630–1640 cm^{-1}. These components would be attributed to β-sheet structures, which in pure proteins exhibit several narrow bands in this range (Surewicz *et al.*, 1993). The component at 1664 cm^{-1} is attributed to β-turns, and the component at 1685 cm^{-1} is probably of mixed β-sheet and β-turn origin.

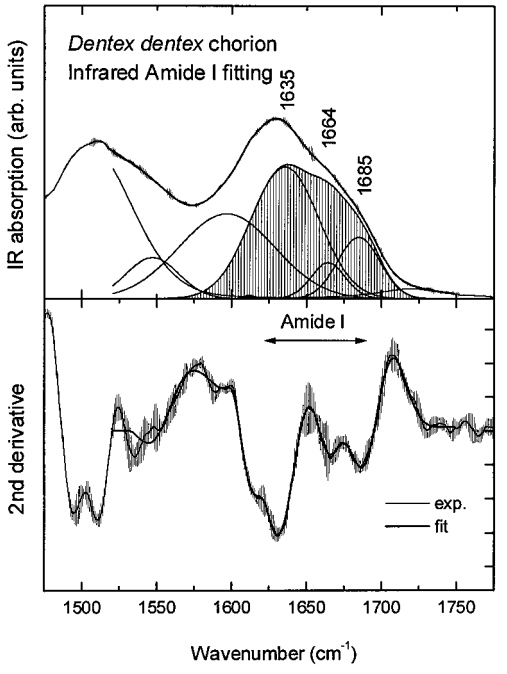

FIG. 6. *Dentex dentex* ATR FT-IR spectral deconvolution in the range 1525–1750 cm^{-1}. Experimental (—) and reconstructed (—) spectra are compared in both the absorption and the second derivative formalisms. The error bars correspond to the experimental data (cf. Fig. 4). The shaded areas are the convolutions of the component bands attributed to amide I vibrations. For details see text.

The relative areas of these bands, normalized to the total amide I intensity, are ca. 70, 10, and 20%, respectively. Overall, the relative infrared area of sheet vs turns in the amide I range is ca. 80:20. The infrared molar absorptivity ratio of these conformations ranges between 2.1 and 3 according to de Jongh *et al.* (1996). Taking an average value of these ratios close to 2.5, the relative infrared area of β-sheet vs turns leads to a 60% β-sheet, 40% β-turn conformation. The error of this determination is on the order of $\pm$10%, because of our assumption that the area of unresolved components equals that of their envelope and also because of the uncertainty in the relative extinction coefficients.

DISCUSSION

Spectral acquisition by ATR FT-IR and FT-Raman spectroscopy coupled with a combination of derivatization and deconvolution procedures has been shown to yield rich information on the secondary structure of fish chorion proteins, without the drawbacks associated with the more conventional vibrational techniques. Unfortunately, this information cannot be fully deciphered in the present investigation of the *D. dentex* chorion proteins due to the lack of equally detailed reference and calibration data. It is hoped that this approach will be most valuable in probing subtle variations of protein secondary structure as a function of primary structural alterations, aging, thermal treatment, etc.

It might be argued that the drying process of *D. dentex* chorions by an infrared-emitter bulb leads to a situation that does not reflect a physiological state. In the case of *D. dentex* as well as in our previous work on *S. gairdneri* (Hamodrakas *et al.*, 1987) and other lepidoptera chorions (*Antheraea polyphemus, Bombyx mori, Mauduca sexta;* Hamodrakas, 1992 and references therein) the effects of air-drying and of drying under an infrared bulb (for 3–4 s) could not be discerned as different by any of the techniques used to monitor secondary structure, including X-ray diffraction. The latter drying process simply leads to better quality spectra. Taking into account that no structural changes were observed during Raman acquisition, which was performed over ca. 10 h in 1-h time intervals under a NIR laser and also the short (3–4 s) exposure times used for drying, it is expected that this procedure simply removes water from the pore canals that traverse fish chorions and not any water trapped between chorion proteins. Therefore, it should not affect their *in vivo* conformation. However, the protein–water interactions in fish and also lepidoptera chorions are largely unexplored and certainly deserve further attention.

Despite the uncertainties associated with the various ways of quantifying secondary structure from the vibrational spectra, it is quite evident that the *D. dentex* chorion consists of proteins that adopt primarily an antiparallel β-pleated sheet conformation, with a strong contribution from β-turns and, perhaps, a minor participation of random segments. This structural picture is similar to that deduced for the egg chorions of *S. gairdneri* (Papadopoulou *et al.*, 1996). Therefore, our findings strengthen the assumption that the common morphological features of the teleostean fish chorions originate from simi-

TABLE III

Results of Infrared Spectral Deconvolution in the Range 1600–1700 cm^{-1}

Position (cm^{-1})	Width (cm^{-1})	Integral	Relative area (%)	Assignment
1597	75.4	1.162		
1612	9.9	0.006		Tyr
1636	*53.3*	*1.277*	69.7	β-sheet
1664	*26.7*	*0.184*	10.0	β-turns
1685	*33.4*	*0.373*	20.3	β-sheet/β-turns
			100.0	

Note. Amide I components are in italics. For details see text.

larities in secondary structure of their constituent proteins (Hamodrakas, 1992).

Still, the formation of these chorions as a self-assembly process is far from being understood. To envisage how these β-sheets interact to form a three-dimensional helicoidal architecture requires also a good knowledge of the corresponding amino acid sequences. Unfortunately, to date, sequences of fish chorion proteins are not available.

Financial support of this work was provided by the Greek General Secretariat of Research and Technology (Grant 99ED8), the University of Athens, and the National Hellenic Research Foundation.

REFERENCES

Bandekar, J., and Krimm, S. (1979) Vibrational analysis of peptides, polypeptides and proteins: Characteristic amide bands of β-turns, *Proc. Natl. Acad. Sci. USA* **76,** 774–777.

Bouligand, Y. (1972) Twisted fibrous arrangements in biological materials and cholesteric mesophases, *Tissue Cell* **4**(2), 189–217.

Bouligand, Y. (1978a) Cholesteric order in biopolymers, *A.C.S. Symp. Ser.* **74,** 237–247.

Bouligand, Y. (1978b) Liquid crustalline order in biological materials, *in* Blumstein, A. (Ed.), Liquid Crystalline Order in Polymers, pp. 261–297, Academic Press, New York/San Francisco/London.

Cai, S., and Singh, B. R. (1999) Identification of β-turn and random coil amide III infrared bands for secondary structure estimation of proteins, *Biophys. Chem.* **80,** 7–20.

Carey, P. R. (1982) Biochemical Applications of Raman and Resonance Raman Spectroscopies, Academic Press, New York.

Carey, P. R., and Salares, V. R. (1980) Raman and resonance Raman studies of biological systems, *in* Clark, R. J. H., and Hester, R. E. (Eds.), Advances in Infrared and Raman Spectroscopy, Vol. 7, pp. 1–58, Heyden, London.

Chen, M., Lord, R. G., and Mendelsohn, R. (1973) Laser-excited Raman spectroscopy of biomolecules. IV. Thermal denaturation of aqueous lysozyme, *Biochim. Biophys. Acta* **328,** 252–260.

de Jongh, H. H. J., Goormaghtigh, E., and Ruysschaert, J. M. (1996) The different molar absorptivities of the secondary structure types in the Amide I region: An attenuated total reflection infrared study on globular proteins, *Anal. Chem.* **242,** 95–103.

Dousseau, F., and Pézolet, M. (1990) Determination of the secondary structure of proteins in acqueous solutions from Amide I and Amide II infrared bands. Comparison between classical and partial least-square methods, *Biochemistry* **29,** 8771–8779.

Edwards, H. G. M., Hunt, D. E., and Sibley, M. G. (1998) FT-Raman spectroscopic study of keratotic materials: Horn, hoof and tortoiseshell, *Spectrochim. Acta Part A* **54,** 745–757.

Fink, D. J., and Gendreau, R. M. (1984) Quantitative surface studies of protein adsorption by infrared spectroscopy. I. Correction for bulk concentrations, *Anal. Biochem.* **139,** 140–148.

Frushour, B. J., and Koenig, J. L. (1975) Raman spectroscopy of proteins, *in* Clark, R. J. H., and Hester, R. E. (Eds.), Advances in Infrared and Raman Spectroscopy, Vol. 1, pp. 35–97, Heyden, London.

Fu, F-N., De Oliveira, D. B., Trumble, W. R., Sarkar, H. K., and Singh, B. R. (1994) Secondary structure estimation of proteins using the Amide III region of Fourier transform infrared spectroscopy: Application to analyze calcium-binding-induced structural changes in calsequestrin, *Appl. Spectrosc.* **48**(11), 1432–1441.

Goormaghtigh, E., Cabiaux, V., and Ruysschaert, J. M. (1990) Secondary structure and dosage of soluble and membrane proteins by attenuated total reflection Fourier transform infrared spectroscopy on hydrated films, *Eur. J. Biochem.* **193,** 409–420.

Griebenow, K., Santos, A. M., and Carrasquillo, K. G. (1999) Secondary structure of proteins in the amorphous dehydrated state probed by FTIR spectroscopy. Dehydration-induced structural changes and their prevention, *Internet J. Vibr. Spectr.* **3**(1), 1–34.

Grierson, J. P., and Neville, A. C. (1981) Helicoidal architecture of fish eggshell, *Tissue Cell* **13**(4), 819–830.

Hamodrakas, S. J. (1992) Molecular architecture of helicoidal proteinaceous eggshells, *in* Case, S. T. (Ed.), Results and Problems in Cell Differentiation, Vol. 19, Chap. 6, pp. 115–186, Springer Verlag, Berlin.

Hamodrakas, S. J., Kamitsos, E. I., and Papanicolaou, A. (1984) Laser-Raman spectroscopic studies of the eggshell (chorion) of *Bombyx mori, Int. J. Biol. Macromol.* **6,** 333–336.

Hamodrakas, S. J., Kamitsos, E. I., and Papadopoulou, P. G. (1987) Laser-Raman and infrared spectroscopic studies of protein conformation in the eggshell of the fish *Salmo gairdneri, Biochim. Biophys. Acta* **913,** 163–169.

Haris, P. I., and Chapman, D. (1995) The conformational analysis of peptides using Fourier transform IR spectroscopy, *Biopolymers* **37,** 251–263.

Jacobs, D. A. H., (1977) "The State of the Art in Numerical Analysis," Chap. II. 2, Academic Press, London.

Jackson, M., and Mantsch, H. H. (1995) The use and misuse of FTIR spectroscopy in the determination of protein structure, *Crit. Rev. Biochem. Mol. Biol.* **30**(2), 95–120.

Jakobsen, R. J., and Wasacz, F. M. (1990) Infrared spectra—Structure correlations and absorption behavior for helix proteins, *Appl. Spectrosc.* **44**(9), 1478–1490.

Kim, H. S., Hartgerink, J. D., and Ghadiri, M. R. (1998) Oriented self-assembly of cyclic peptide nanotubes in lipid membranes, *J. Am. Chem. Soc.* **120,** 4417–4424.

Krimm, S., and Bandekar, J. (1986) Vibrational spectroscopy and conformation of peptides, polypeptides, and proteins, *Adv. Prot. Chem.* **38,** 181–386.

Lee, D. C., Haris, P. I., Chapman, D., and Mitchell, R. C. (1990) Determination of protein secondary structure using factor analysis of infrared spectra, *Biochemistry* **29,** 9185–9193.

Neville, A. C. (1975) Biology of the Arthropod Cuticle, Springer-Verlag, Berlin/Heidelberg/New York.

Neville, A. C. (1981) Cholesteric proteins, *Mol. Cryst. Liq. Cryst.* **76,** 279–286.

Neville, A. C. (1986) The physics of helicoids: Multidirectional "plywood" structures in biological systems, *Phys. Bull.* **37,** 74–76.

Orfanidou, C. C., Hamodrakas, S. J., Chryssikos, G. D., Kamitsos, E. I., Wellman, S. E., and Case, S. T. (1995) Spectroscopic studies of *Manduca sexta* and *Sesamia nonagrioides* chorion protein structure, *Int. J. Biol. Macromol.* **17**(2), 93–98.

Papadopoulou, P., Galanopoulos, V. K., and Hamodrakas, S. J. (1996) Molecular and supramolecular architecture of the *Salmo gairdneri* proteinaceous eggshell during development, *J. Struct. Biol.* **116,** 399–412.

Sarver, R. W., and Krueger, W. C. (1991a) Protein secondary

structure from Fourier transform infared spectroscopy: A data base analysis, *Anal. Biochem*. **194,** 89–100.

Sarver, R. W., and Krueger, W. C. (1991b) An infrared and circular dichroism combined approach to the analysis of protein secondary structure, *Anal. Biochem*. **199,** 61–67.

Savitsky, A., and Golay, M. J. E. (1964) Smoothing and differentiation of data by simplified least-squares procedures, *Anal. Chem*. **36,** 1627–1639.

Schultz, G. E., and Schirmer, R. H. (1978) Principles of Protein Structure, Springer Verlag, New York.

Singh, B. R., and Fuller, M. P. (1991) FT-IR in combination with the attenuated total reflectance technique: A very sensitive method for the structural analysis of polypeptides, *Appl. Spectrosc.* **45**(6), 1017–1021.

Singh, B. R., Fuller, M. P., and Schiavo, G. (1990) Molecular structure of tetanus neurotoxin as revealed by Fourier transform infrared and circular dichroic spectroscopy, *Biophys. Chem*. **46,** 155–166.

Spiro, T. G., and Gaber, B. P. (1977) Laser-Raman scattering as a probe of protein structure, *Annu. Rev. Biochem*. **46,** 553–572.

Surewicz, W. K., Mantsch, H. H., and Chapman, D. (1993) Determination of protein secondary structure by Fourier transform infrared spectroscopy: A critical assessment, *Biochemistry* **32**(2), 389–394.

Susi, H., and Byler, D. M. (1986) Resolution-enhanced Fourier transform Infrared spectroscopy of enzymes, *Methods Enzymol.* **130,** 290–311.

Venyaminov, S. Y., and Kalnin N. N. (1990a) Quantitative IR spectrophotometry of peptide compounds in water (H_2O) solutions. I. Spectral parameters of amino acid residue absorption bands, *Biopolymers* **30,** 1243–1257.

Venyaminov, S. Y., and Kalnin, N. N. (1990b) Quantitative IR spectrophotometry of peptide compounds in water (H_2O) solutions. II. Amide absorption bands of polypeptides and fibrous proteins in α-, β-, and random coil conformations, *Biopolymers* **30,** 1259–1271.

Williams, R. W. (1986) Protein structure analysis using Raman amide I and amide III spectra, *Methods Enzymol.* **130,** 311–331.

Williams, R. W., and Dunker, A. K. (1981) Determination of the secondary structure of proteins from the amide I band of the laser-Raman spectrum, *J. Mol. Biol.* **152,** 783–813.

Yu, N. T. (1977) Raman spectroscopy: A conformational probe in biochemistry, *CRC Crit. Rev. Biochem*. **4,** 229–280.